Discrete Element Modelling of Crushable Tube-Shaped Grains

M. Stasiak, G. Combe, V. Richefeu, P. Villard, J. Desrues, G. Armand, and J. Zghondi

Abstract This study focuses on highly compressible granular material incorporated in novel tunnel-lining technology, precisely, the prefabricated tunnel segments called voussoirs. The material composed of hollow, brittle, tube-shaped particles were designed such that the crushing of the constituent particles results in high material compressibility. This paper is essentially dedicated to discrete-element simulations that involve both the breakage of the particles at micro scale and the resulting effects on macro scale. Firstly, a 3D model was proposed in order to adequately reflect the complex geometry and the breakage manner. In applied strategy, the tube-shaped particle is modelled as a cluster of bonded, rigid, sphero-polyhedral sectors. Then, the identification of the parameters that control the mechanical response and the strength of the particles is presented using a radial compression test. This step was supported by laboratory experimental tests. Finally, six assemblies of cluster under oedometric loading were studied by means of Discrete Element numerical simulations. We analysed the influence of the sample size on the evolution of particles breakage and void ratios. This analysis resulted in the definition of new framework for void ratio and a model capable of predicting breakage as a function of the strains.

Keywords DEM · Sphero-polyhedral particles · Cluster model · 3D simulations · Grain crushing · Oedometric compression

---

This research was complete at the 3SR Laboratory of the University of Grenoble. 3SR-Lab is part of the LabEx Tec 21 (Investissements d'Avenir, Grant Agreement No. ANR-11- LABX-0030).

M. Stasiak (✉) · G. Combe · V. Richefeu · P. Villard · J. Desrues
Univ. Grenoble Alpes, CNRS, Grenoble INP (Institute of Engineering Univ. Grenoble Alpes), 3SR, Grenoble, France
e-mail: marta.stasiak@3sr-grenoble.fr; gael.combe@3sr-grenoble.fr; vincent.richefeu@3sr-grenoble.fr

G. Armand · J. Zghondi
Andra, R&D Division, Meuse/Haute-Marne Underground Research Laboratory, Bure, France

P. Giovine et al. (eds.), *Micro to MACRO Mathematical Modelling in Soil Mechanics*, Trends in Mathematics, https://doi.org/10.1007/978-3-319-99474-1_35

1 Introduction

A number of studies shown that grain fragmentation plays an important role in various processes like grinding (clinker grinding in cement industry [1], wheat grinding [2]), powder compaction [3], civil engineering works (grain crushing in pile installation and cyclic solicitation [4–6]), etc. The characterisation of grain crushing is a fundamental step to understand the mechanics of such granular materials. The study presented in that paper is dedicated to mechanical characterisation of a novel, specifically manufactured granular material which is characterised by a double porosity and that is incorporated in technology of the tunnel lining [7].

To prevent the high stresses on the tunnel lining triggered by the decompression and creep of the hosted rock, an additional compressible granular layer is added at the interface rock–lining, this is, at the extrados of the concrete segments. That original compressible segment is called VMC (Voussoir Monobloc Compressible, US Patent pending) and was jointly developed by CMC (a consulting company) and Andra. The compressible layer between concrete lining and surrounding rock spreads stresses by means of load transfer mechanisms [8]. When the stress applied by the rock becomes locally very high, the granular material adapts by large contact force rearrangements. To this end, the granular material must show high compressibility abilities. Then, a novel manufactured granular material was designed: it consists of crushable, tube-shaped particles made of backed clay (called shells); Fig. 1a. This specific application takes advantage of a high internal porosity of the shell. Therefore, the compressibility is tightly connected with grain crushing presented herein.

The full mechanical behaviour of such new voussoir technologies needs to be investigated aiming its improvement and optimisation. For that purpose, we first focus on the study of the micro-mechanical behaviour of the granular layer made of shells. Many laboratory tests were performed to explore the strength and the strain capability of large assemblies of shells—oedometer and triaxial compression tests [9]. Although the experimental campaigns have already provided valuable data, the optimisation of the mechanical strength of this granular material needs to be investigated at the inter-granular contact scale. The Discrete Element Method

Fig. 1 (**a**) An intact shell (backed clay), (**b**) broken shell after an oedometeric compression, $\sigma_a = 420\,\mathrm{kPa}$

(DEM) [10] was chosen as a numerical approach that enables the understanding of the micro-mechanical behaviour of this specific material, at the grain scale.

Among all existing numerical strategies capable of modelling particle breakage, two are frequently used. First strategy takes into consideration particles that are replaced by smaller ones when the breakage occurs—that is, when a given limit stress criterion is satisfied [11, 12]. In the second approach, the particle is generated as a set of smaller particles connected together by means of bonding forces acting up to a given yield strength criterion. As an example, [13, 14] modelled grains of silica sand as an agglomerates of spheres that can be separated. Models based on polygonal shapes have also been proposed by [11, 15]. Figure 1b presents the manner of breakage for shells in an assembly subjected to oedometric compression. It can be observed that shells are sliced in longitudinal parts following radial plans. Hence, in this study, we will use bonded sphero-polyhedral shapes (polygonal shapes made of tubes for edges, spheres for corners and plains).

In that paper, we firstly present our DEM model used to simulate the fracture behaviour of a tube-shaped particle. A validation of the grain model is supported by an experimental campaign presented in [16] and briefly recalled in that article. Finally, we present results and analysis of six different samples under oedometric loading focusing on the quantification of breakage and void–solid ratio defined in standard and nonstandard frameworks.

2 Discrete Element Model

Discrete Element Method (DEM) is a particle-scale numerical method commonly used to reflect the behaviour of granular materials [17–19]. It operates on the *Newton*'s second law that is discretised in time and solved by means of a given numerical integration scheme [20]. *Newton*'s equations require the knowledge of the contact forces acting between rigid bodies. The commonly used concept relates the contact force with local kinematic parameters (overlap, relative velocities, etc.) between two particles. The trend between overlap and force is described by the force laws, discussed in more details in this section. The model description is followed by the identification and validation of model parameters.

2.1 Tube-Shaped Breakable Particles

Numerically, a cluster of 3D bonded sectors forms a tube-shaped particle as shown in Fig. 2a. A sector is itself composed of sub-elements (spheres, tubes and thick planes) with no relative movement; it can be considered as a rigid body. Within one cluster, the sectors are bonded through four adjacent spheres; Fig. 2b. These bonds act elastically in the two directions related to the opening of the common plane

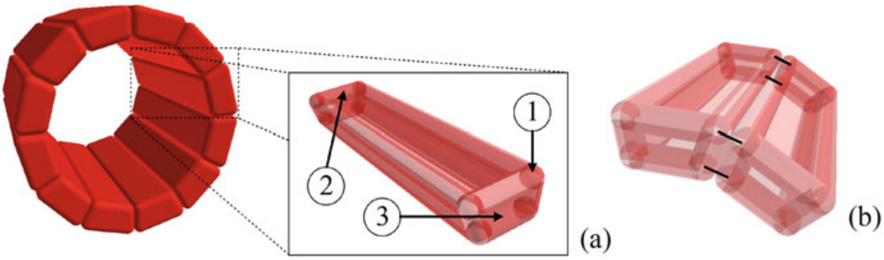

Fig. 2 (**a**) A tube-shaped particle modelled as a cluster of 12 sphero-polyhedral elements called sectors. A sector is a rigid body composed of sub-elements of 3 types: ① spheres as corners, ② tubes as edges and ③ thick planes as faces; (**b**) sectors glued with 4 bonded contact (black lines) through 4 spheres

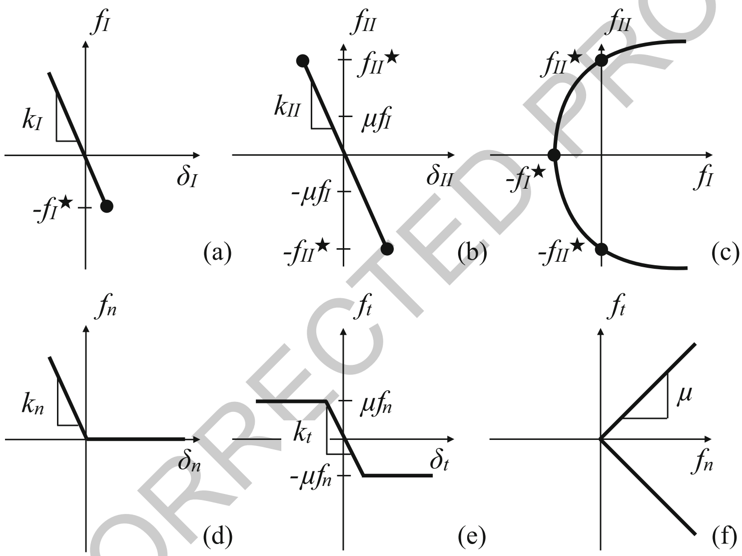

Fig. 3 Force laws for bonded links (top row) and for cohesionless frictional contacts (bottom row) respectively: (**a**)/(**d**) loading in mode-I/normal direction, (**b**)/(**e**) loading in mode-II/tangential direction, and (**c**)/(**f**) failure/Coulomb criterion

(joined faces) as in fracture modes I and II. The elastic relation is written formally:

$$\begin{pmatrix} f_I \\ f_{II} \end{pmatrix} = \begin{pmatrix} k_I & 0 \\ 0 & k_{II} \end{pmatrix} \cdot \begin{pmatrix} \delta_I \\ \delta_{II} \end{pmatrix} \tag{2.1}$$

In a pure mode-I loading (tensile loading), the elastic force normal to the plane cannot exceed a threshold force $f_I^\star$; Fig. 3a. For a pure mode-II loading (shear loading), a tangential elastic force withstands if it is in the range of $\pm f_{II}^\star$; Fig. 3b.

When modes I and II are activated at once, a bond holds as long as a yield function φ remains negative, with:

$$\varphi = \frac{-f_I}{f_I^\star} + \left(\frac{|f_{II}|}{f_{II}^\star}\right)^q - 1, \tag{2.2}$$

where q is a numerical parameter that controls the shape of the function, as suggested by Delenne [21]. The yield function φ in the f_I–f_{II} plane is shown in Fig. 3c for a given value of q. In this model, the mechanical behaviour of a cluster is elastic and brittle, but the involved mechanical parameters (stiffnesses and threshold forces) and the fracture pattern are related to the initial slicing of the cluster; Fig. 2.

As soon as $\varphi \geq 0$ for one of the four bonds between two sectors, the four bonds are broken. Not bonded contacts (never glued or broken bonds) are ruled by normal and tangential laws. The normal contact force $f_n = k_n\,\delta_n$ is ruled by a linear and elastic law, where k_n is the normal stiffness of the contact and δ_n the normal distance overlap in the contact. The tangential force f_t results from an accumulation of increments $\Delta f_t = k_t\,\Delta U_t$, where k_t is a tangential stiffness and ΔU_t is the relative tangential displacement in contact. f_t is limited to $\pm\mu f_n$, where μ is the *Coulomb* coefficient of friction. Notice that the frictional contact law is also used between the clusters inside the assembly.

In DEM, energy dissipation is always a matter of concern [19]. Energy dissipation can be managed through various mechanisms. The *Coulomb* friction is one of the possible mechanisms. Additionally, we used two other dissipation model: (1) a viscous damping that act in addition to normal elastic forces, and (2) a numerical damping that affects artificially the resultant forces of the rigid bodies, like in [17]. Both damping strategies are, in the context of quasistatic loadings, only used to increase dissipation efficiency, especially when the clusters break (particles breakage release a lot of energy that must be dampen for sake of numerical stability). For all simulations presented here, we took advantage of the velocity Verlet [20] numerical scheme implemented in a parallelised tool named `Rockable`, developed by *Vincent Richefeu* from the GéoMécanique group of 3SR Lab. (Univ. Grenoble Alpes, France).

2.2 *Identification of the DEM Parameters*

Our discrete model includes two sets of mechanical parameters: the first set for the laws that bonds sectors of breakable clusters (k_I, k_{II}, $f_I^\star$, $f_{II}^\star$ and q; Fig. 3a–c), and the second one for laws ruling no cohesive–frictional contacts (k_n, k_t, μ; Fig. 3d–f).

▹ **Bonded Sectors**

As observed in Fig. 1b, the shells break into stick-shaped parts. As well, a radial compression on a single shell produces stick-shaped parts at breakage when it is performed experimentally at the laboratory. Such test (inset of Fig. 4a) allows

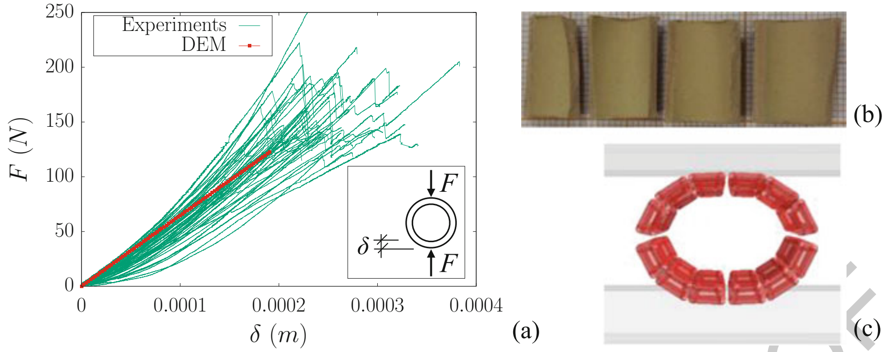

Fig. 4 (**a**) Force–displacement curves of 83 radial compression tests. Inset: the loading condition where the displacement δ is imposed at constant velocity $\dot{\delta} = 0.01$ m/s; (**b**) shells subjected to radial compression most often break in 4 parts sliced in the radial planes; (**c**) a simulation that reflects a typical manner of shells breakage

to assess a rupture force F and a corresponding rupture displacement δ for the shell. Hence, 83 tests were carried out on shells. Due to material and geometrical imperfection, a strong variability was observed in the mechanical response, Fig. 4a. In most cases, it was experimentally observed that the grains break into 4 parts separated by the vertical and horizontal planes.

With our numerical model, the elasticity of the shell structure F/δ is controlled by the elastic parameters of bonded links (k_I, k_{II}) for which the order of magnitude needs to be estimated (for a given number of sectors used to discretise the shell shape). The parameters $f_I^\star$ and $f_{II}^\star$, and the shape parameter q that control the rupture force F for a given shell geometry, also need to be estimated.

The number of sectors used to discretise a shell needs to follow few requirements: circular shape of the shell; ability to break in 4 parts for radial compression; the smallest number of sectors as possible to shorten computation time. To fulfil these requirements, we used 12 sectors per clusters; as shown in Fig. 2.

A number of simulations allowed us, by means of trials and errors, to select the right stiffnesses k and yield forces $f^\star$. The yielding force $f_I^\star$, in fracture mode I, leading to the experimental mean macroscopic force at rupture was found in the order of 85 N. A statistical analysis of these forces clearly shows a Weibull distribution [16]. The associated stiffness k_I was set equal to 5.5×10^6 N/m in order to target a mean experimental elastic slope. The force-displacement relation modelled by DEM is shown in Fig. 4a (red line). The yielding force $f_{II}^\star$, in fracture mode II, has no influence on the force F at shell rupture. We thus selected the non-definitive value of 50 N on the basis of an analysis of its influence on the mechanical response of the shell. k_{II} was set equal to k_I.

Finally, the parameters q in the yield equation (Eq. (2.2)) was arbitrarily set to 2 (increasing this value made no marked changes).

▹ **Cohesionless Frictional Contacts**

As seen in Sect. 2.1, particles interact with each other through their contact points. At each contact point, a normal elastic compressive force and an incremental tangential force (with a *Coulomb* threshold) are computed. Both contact laws need stiffnesses, k_n and k_t, that are found to be the same in the literature [10]. The normal stiffness k_n was estimated using the Young modulus E of backed clay (for brick, $E = 14\,\text{GPa}$). Assuming that the *Poisson* coefficient of backed clay is $\nu = 0.3$, it can be shown that the dimensionless stiffness parameter of a dense sample of shells submitted to a mean stress of $P = 1\,\text{MPa}$ is $\kappa \simeq 400$ [10]. Assuming an elastic normal contact law, $\kappa = k_n/(aP)$, where a is the mean size of the particles (0.02 m). This estimation leads to $k_n = 8 \times 10^6$ N/m, which is observed to be of the same order as the value obtained for k_I. Thus, for the sake of simplicity, we arbitrarily used a uniform stiffness coefficient: $k_n = k_t = k_I = k_{II} = 5.5 \times 10^6$ N/m.

Other experimental tests enable us to assess a friction coefficient between two curved lateral surfaces of the grains: 0.24 ± 0.06.

3 Oedometer Tests

Using a particle model that reliably reflects its mechanical response and breakage at the grain scale, we enlarged the scale of interest to investigate mechanical behaviour of an assembly of the crushable clusters. A number of samples was prepared varying mechanical parameters in order to reproduce real sample; Sect. 3.1. An oedometer (uniaxial compression) test is commonly used to study compressible properties of the materials in geo-mechanics, therefore, Discrete Element simulations of this test were performed for this novel granular material; Sect. 3.2. The material (backed clay) does not show significant compressible properties itself, but tube-shape geometry of the particles provides a high compressibility to the assembly thanks to the particle collapse at breakage. Hence, by analysing mechanical behaviour of samples a special attention is paid to the evolutions of void ratio and breakage rate during oedometric compression; Sect. 3.3.

3.1 Sample Preparation

The sample was built by depositing under gravity the clusters into a cylindrical box. The number density n (number of clusters per unit volume) was chosen as reference parameters to be compared with an experimental measurement. Note that during that procedure $f^{\star}_{I,II}$ were increased such that clusters cannot break. The procedure consists of two steps: gravity deposit and numerical relaxation phase. A number of clusters were distributed on the cylindrical grid such that there was no possible interaction between them. The orientation of clusters was random. Then, the gravity accountable for the vertical movement was activated. Simultaneously, the assembly

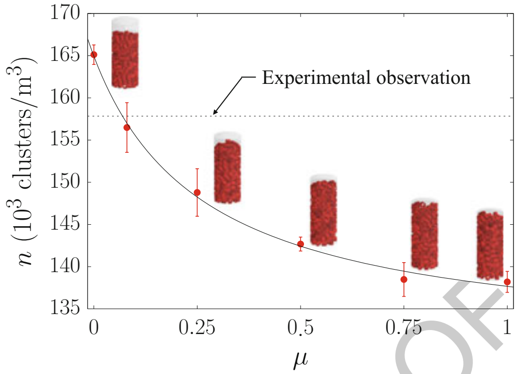

Fig. 5 Trend (solid line) between number density n and friction coefficient μ between clusters. The points are the mean values with corresponding standard deviation showing the variability of five different simulations for each value of μ used

was shaken by means of an initial velocity assigned separately to each cluster with random direction but constant magnitude of 1 m/s. Once all clusters embed on the bottom of the mould, the sample rested until the equilibrium state was reached, which was verified in terms of low kinetic energy. Numerically, the number density n can be controlled by varying the coefficient of friction acting between the clusters.

Figure 5 shows the obtained trend that describes n as a function of intergranular friction coefficient for a sample made of 333 clusters. For friction $\mu \simeq 0.08$, the number density n reached the experimental one ($n = 157\,840$ clusters/m^3); therefore, it was used for sample preparation.

3.2 *Oedometric Compression Test Procedure*

The oedometer tests were performed with an imposed velocity of the upper plate, $v = 0.05$ m/s. To insure quasi-static evolution of a granular assembly during its compression, the inertial number criterion [10] was considered. It has been shown that $I < 10^{-3}$ the mechanical behaviour of the granular assembly is stain-rate independent [22]. In this study, v was chosen such that I was of the order of 10^{-4}.

Whereas the intergranular friction coefficient μ was set to 0.08 in the sample deposit phase in order to obtain the right density, it was switched to its nominal value $\mu = 0.30$ for the oedometric compression.

3.3 *Results*

DEM simulations of oedometric tests were performed for samples with different sizes, varying either the diameter or the height of the sample. Six samples of different sizes (referred to as their sizes: diameter $D\times$ height h_0) were tested; the number of clusters ranged from 203 to 1926. In Table 1, one can observe that

Table 1 Initial state of samples described by the diameter of sample D, the height of sample h_0, the number density n, and the void ratios e and $e^{\star}$; Eq. (3.2)

No.	No. shells/no. sectors	$D \times h_0$ (cm)	n (clusters/m^3)	$e^{\star}$	e
1	1926/23,112	35 × 12.2	164,139	0.579	2.423
2	1579/18,948	35 × 10.1	162,717	0.593	2.453
3	1105/13,260	35 × 07.3	156,479	0.656	2.591
4	790/9480	35 × 05.1	160,965	0.610	2.490
5	1047/12,564	25 × 13.1	163,068	0.589	2.445
6	203/2436	11 × 13.5	158,800	0.632	2.538

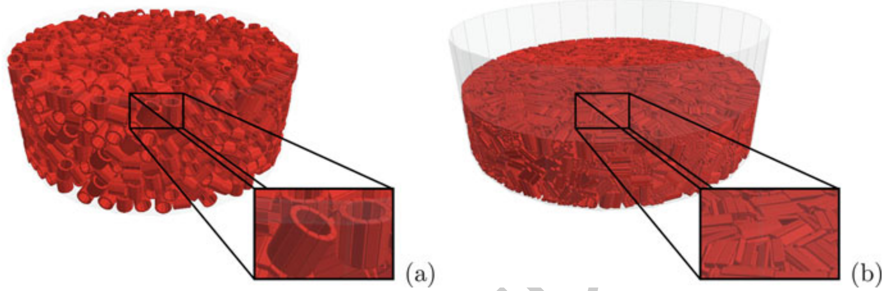

Fig. 6 Sample made of 1926 cluster, that is, 23,112 sectors or 600,912 sub-elements: (**a**) before oedometric compression—all grains are intact, (**b**) the end of test for $\varepsilon_a = 60\%$ and $\sigma_a = 18.17$ MPa—all grains are crushed

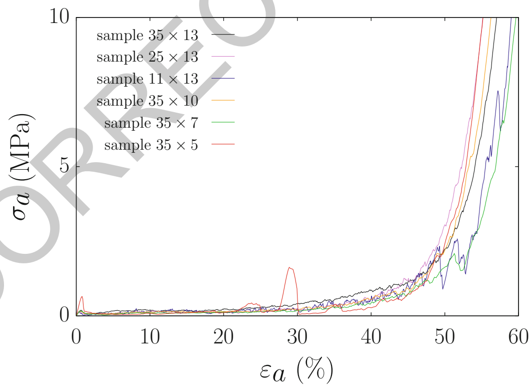

Fig. 7 Mechanical response for oedometric loading. Comparison between cylindrical samples with various sizes $D \times h_0$ (cm)

although all the samples were prepared with the same protocol, their density number depends on their sizes. This observation can be related to a very common rigid boundary effect [10].

In Fig. 6 one can see an example of a sample before (Fig. 6a) and after (Fig. 6b) an oedometric compression. Figure 7 shows the stress–strain relationship with different

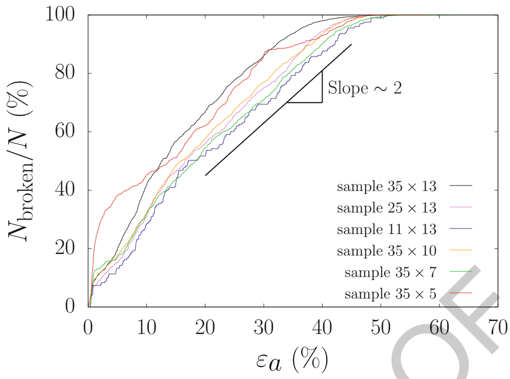

Fig. 8 Evolution of damage defined as the rate of broken bonds for cylindrical samples with various sizes $D \times h_0$ (cm)

sample sizes, by using the *Hencky* definition of the vertical strain $\varepsilon_a = \log(h/h_0)$. It is remarkable to observe that, as reported in the experiments [9], the stress-strain curve does not show any significant dependence on the number of clusters neither on the diameter–high ratio.

One of the advantages of DEM is that quantities can be assessed at the grain scale; it means that grain breakage can accurately be followed during the compression test. Figure 8 reports the proportion of broken clusters N_{broken}/N with respect to the vertical strain. After an initial transient regime, one can observe that for $\varepsilon_a \in [15\%\ 40\%]$, the breakage is independent of the sample size and it rises at a constant rate of 2 (percentage of newly broken clusters per percentage of vertical strain). Once all the initial bonds are broken, $\varepsilon_a \geq 50\%$, the sample becomes dense and the loading starts to increase rapidly; Fig. 7.

The compressibility of the samples derives from the large amount of free space, i.e., internal cluster voids. Due to its specific shape (Fig. 2), each cluster presents an internal void that represent 51% of the total volume of a cluster. Considering the volume of the sample V_{tot} and the volume of the solid phase V_{s} (sum of the volume of sectors), the classical definition of void ratio

$$e = (V_{\mathrm{tot}} - V_{\mathrm{s}})/V_{\mathrm{s}} \tag{3.1}$$

leads to high values: $e \in [2.423; 2.591]$. The peculiar geometry of a cluster disables access to the space trapped inside it while it remains intact. Once the cluster is broken the trapped space is released. Thus, we considered another definition for the void ratio, where $V_{\mathrm{accessible}}$ are all the available space in the sample and $V_{\mathrm{inaccessible}}$ is the space that cannot be filled by matter because of geometric exclusions (inside intact clusters). In that way, the geometric exclusions are accounted for:

$$e^{\star} = \frac{V_{\mathrm{accessible}}}{V_{\mathrm{inaccessible}}} = \frac{V_{\mathrm{tot}} - (V_{\mathrm{s}} + V^{\star})}{V_{\mathrm{s}} + V^{\star}} \tag{3.2}$$

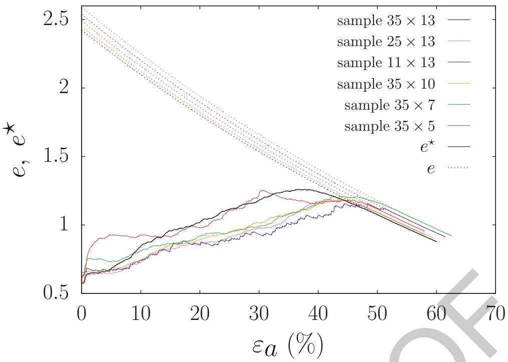

Fig. 9 Void ratios' evolution with respect to axial strain. Comparison between cylindrical samples with various sizes (D cm$\times h_0$ cm), where $e^\star$ is defined by modified criterion; Eq. (3.2)

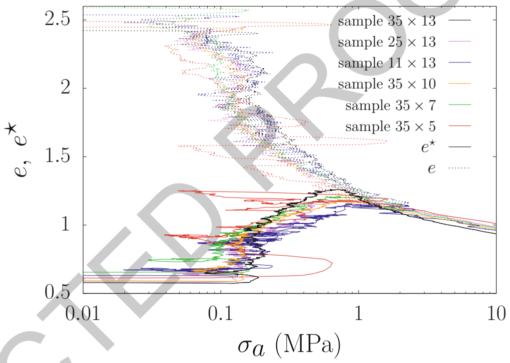

Fig. 10 Evolution of void ratios e and $e^\star$ (Eq. (3.2)) with respect to axial stress for six cylindrical samples with various sizes $D \times h_0$ (cm)

where $V^\star$ is the volume of the hollow part of intact clusters. In Figs. 10 and 9, the evolution of both standard (e) and non-standard ($e^\star$) void ratios are plotted as a function of axial stress and strain. The standard void ratio e decreases non-linearly, simply due to the logarithm definition of strain, Fig. 9. Solid lines present non-standard void ratio $e^\star$ which, in all cases, rises up to e in non-monotonous manner. This follows from the fact that the progressive cluster breakage enables access to internal voids along the test. Once all the clusters are crushed, $V^\star = 0$ and thus, Eqs. (3.1) and (3.2) become identical. The evolution of $e^\star$ shown in Fig. 10 is something different from the consolidation curves classically produced for fine soils in the field of geotechnical engineering. Despite similar features, the seeming consolidation slope (that increases with the stress level) relates mainly to different mechanisms related to the collapse of constituent particles. A constitutive macroscopic model dedicated to this mechanism should not be based on e directly but rather on a modified version of this variable, as we suggested by introducing $e^\star$. The derivation of such constitutive model is, however, not our final objective in this study.

Let's now see how the $e^\star$–ε_a plot may include the cluster breaking rate $d = N_{\text{broken}}/N$ by considering it proportional to the axial strain as a first order estimation: $d = 2\varepsilon_a$. By defining the cluster void ratio $E_0 = R^2_{\text{int}}/(R^2_{\text{ext}} - R^2_{\text{int}})$,

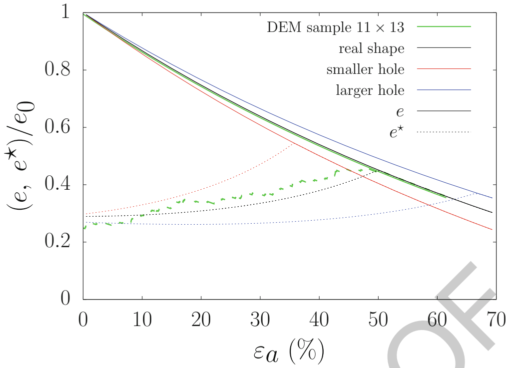

Fig. 11 Evolution of normalised void ratios e/e_0 (solid lines) and $e^\star/e_0$ (dashed lines) with respect to axial strain: (green) simulation with the 11×13 sample, (black) compression curves according to Eq. (3.3), (red) a prediction for shells with smaller holes and $d = 2.5\varepsilon_a$, and (blue) a prediction for shells with larger holes and $d = 1.5\varepsilon_a$

Eq. (3.2) can be re-written as follows:

$$e^\star(d) = \frac{e(\varepsilon_a) - (1-d)E_0}{1 + (1-d)E_0} \quad \text{where} \quad e(\varepsilon_a) = \frac{1+e_0}{\exp(\varepsilon_a)} - 1 \tag{3.3}$$

Note that the logarithmic strain definition is used in the derivation of this formula, and the relation between e and ε_a needs to include the initial void ratio e_0 of the sample. Figure 11 shows e/e_0 as a function of ε_a superimposed on the result of a simulation. Because the relation between e and ε_a is purely geometric, the e-curves fit perfectly (the green curve has been slightly shifted to be evidenced). The evolution of predicted $e^\star$ follows quite well the simulated one showing that the geometric model is actually monitored by the evolution of d with respect to ε_a. It is interesting to note that, in the context of crushable particles that are able to "release" voids, e can be seen as an upper limit for $e^\star(d = 1)$, while the natural definition of void ratio when some voids are enclosed within the particles should be $e^\star(d = 0)$.

One example of the interest of Eq. (3.3) can be illustrated by attempting to predict the oedometric compression behaviour as a function of the hole radius of the shells in order to optimise them. Assuming a faster increase of d for smaller hole radii, the tendencies are shown in Fig. 11 (red and blue curves). Obviously, the reliability of these predictions is questionable because the model still needs to include a proper evolution law for the damage-like parameter d as a function of the pressure for instance.

4 Conclusions

A complex DEM model was proposed to simulate the compression of crushable tube-shaped grains. The specific geometry was successfully represented by clusters of 3D bonded sectors modelled with sphero-polyhedron. It allowed the particles to behave elastically up to their brittle rupture into smaller parts. Both an experimental campaign on tube-shaped grains (shells) and the numerical trials enabled us to identify the mechanical parameters required for correct reflection of elastic and brittle fracture of a single grain.

At macro-scale, oedometer test compressions were conducted numerically for cylindrical samples of various sizes. These simulations demonstrated the model ability to capture the collapse mechanisms at the particle scale. Negligible influence of sample's size and related boundary effects was observed on the mechanical response. The void ratio was redefined in the context of voids that can be temporarily inaccessible, before the particle collapse. In each test, the evolution of some data, known as difficult to assess in experiments, has been reported. In particular, the rate of breakage and the void ratios have been shown to evolve non-linearly in the course of straining. An analytical model able to describe the evolution of the void ratio $e^{\star}$ with respect to the vertical strain under an oedometric condition was proposed. This model open interesting perspectives to predict the volumetric behaviour when the cluster thickness is changed. A step forward will be to enhance this model to predict the stress behaviour with respect to the vertical strain, taking into account the compression resistance of one single shell. In the future, one objective is to use this numerical model to improve some material parameters (e.g., shell sizes, cement strength between the shells) such that the coupling of compressibility and strength are optimised for the prevention of tunnel convergence.

References

1. Esnault, V.P.B., Roux, J.-N.: 3D numerical simulation study of quasistatic grinding process on a model granular material. Mech. Mater. **66**, 80–109 (2013)
2. Blanc, N., Richefeu, V., Mayer, C., Delenne, J.-Y.: Deconvolution of grading curves during milling: example of wheat straw. EPJ Web Conf. **140**, 13019 (2017)
3. Nguyen, D.-H., Azéma, E., Philippe, S., Radjaï, F.: Bonded-cell model for particle fracture. Phys. Rev. E **91**(2), 022203 (2015)
4. Colliat-Dangus, J.-L.: Comportement des matériaux granulaires sous fortes contraintes: influence de la nature minéralogique du matériau étudié. PhD Thesis, 1986
5. Doreau-Malioche, J., Combe, G., Viggiani, G., Toni, J.-B.: Shaft friction changes for cyclically loaded displacement piles: an x-ray investigation. Géotech. Lett. **8**(1), 1–7 (2018)
6. Yang, Z.X., Jardine, R., Zhu, B., Foray, P., Tsuha, C.: Sand grain crushing and interface shearing during displacement pile installation in sand. Géotechnique **60**(6), 469–482 (2010)
7. Andra's & CMC(a Consulting Company) have jointly developed the COMPRESSIBLE ARCH SEGMENT CONCEPT, called VMC (US patent pending)
8. Chevalier, B., Combe, G., Villard, P.: Experimental and discrete element modeling studies of the trapdoor problem: influence of the macro-mechanical frictional parameters. Acta Geotech. **7**(1), 15–39 (2012)
9. Andra: Internal report (2017)
10. Radjaï, F., Dubois, F.: Discrete-Element Modeling of Granular Materials. Wiley-Iste, London (2011)
11. Cantor, D., Estrada, N., Azéma, E.: New approach to grain fragmentation for discrete element methods. Geomechanics from Micro to Macro (2015). ISBN 978-1-138-02707-7, pp. 257–262
12. Tsoungui, O., Vallet, D., Charmet, J.-C.: Numerical model of crushing of grains inside two-dimensional. Powder Technol. **105**, 190–198 (1999)

13. McDowell, G.R., Harireche, O.: Discrete element modelling of yielding and normal compression of sand. Géotechnique **52**(4), 131–135 (2002)
14. Cheng, Y.P., Nakata, Y., Bolton, M.D.: Discrete element simulation of crushable soil. Geotechnique **53**(7), 633–641 (2003)
15. Nader, F., Silvani, C., Djeran-Maigre, I.: Grain breakage under uniaxial compression, through 3D DEM modelling. EPJ Web Conf. **140**, 07005 (2017)
16. Stasiak, M., Combe, G., Desrues, J., Richefeu, V., Villard, P., Armand, G., Zghondi, J.: Experimental investigation of mode I fracture for brittle tube-shaped particles. EPJ Web Conf. **140**, 07015 (2017)
17. Cundall, P., Strack, O.: A discrete numerical model for granular assemblies. Géotechnique **29**(1), 47–65 (1979)
18. CEGEO: Particle shape dependence in 2D granular media. Europhys. Lett. **98**(4), 44008 (2012)
19. Atman, A.P.F., Claudin, P., Combe, G.: Departure from elasticity in granular players: Investigation of a crossover overload force. Comput. Phys. Commun. **180**(4), 612–615 (2009)
20. Allen, M.P., Tildesley, D.J.: Computer Simulation of Liquids. Oxford Science Publications, Oxford (1987)
21. Delenne, J.-Y.: Milieux granulaires à comportement solide: modélisation, analyse expérimentale de la cohésion, validation et applications. PhD Thesis, 2002
22. GDR Midi: On dense granular flows. Eur. Phys. J. E **14**, 341–365 (2004)